

Regular Article

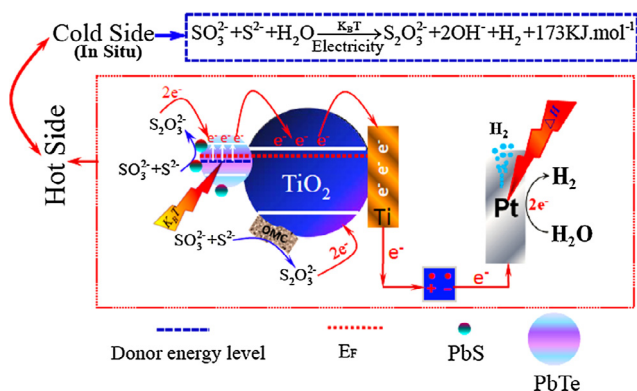
Enhanced hydrogen production of PbTe-PbS/TNAs electrodes modified with ordered mesoporous carbon



Shiyuan Gao, Bin Wang, Zhongqing Liu *

School of Chemical Engineering, Sichuan University, Chengdu 610065, Sichuan, China

GRAPHICAL ABSTRACT



ARTICLE INFO

Article history:

Received 14 April 2017

Revised 1 June 2017

Accepted 6 June 2017

Keywords:

PbTe-PbS

TiO₂ nanotube arrays

Ordered mesoporous carbon

Electrocatalysis

ABSTRACT

PbTe-PbS/TiO₂ nanotube arrays (PbTe-PbS/TNAs) were synthesized by the successive ionic layer adsorption and reaction (SILAR) followed by linear sweep voltammetry (LSV). Using Nafion as a binder, ordered mesoporous carbon was cast on these materials to generate the modified electrodes OMC/PbTe-PbS/TNAs. It was demonstrated that the electrode modification with OMC could enhance the charge transfer between the electrode surface and the electrolyte solution, improve the energy band bending of the electrode/electrolyte interface, increase the active electrochemical surface area of the electrode, and reduce the overpotential of the electrode reactions. Under ambient conditions, the short circuit current density (37.84 mA cm⁻²) and the active electrochemical surface area (29 mF cm⁻²) of the OMC/PbTe-PbS/TNAs electrode were 27.49% and 36.79% higher than that of PbTe-PbS/TNAs (29.68 mA cm⁻² and 21.2 mF cm⁻²), respectively. A particularly important feature of the OMC modification is that the hot electron extraction capability of the PbTe-PbS/TNAs electrode remained in the new system to provide rapid enhancement of short circuit current density upon increasing temperature. The OMC/PbTe-PbS/TNAs electrode registered a hydrogen generation rate of 11 mL cm⁻² h⁻¹, with an energy efficiency of 98.79% and a heat efficiency of 43.03% under cell voltage of 1.0 V at 55 °C.

© 2017 Elsevier Inc. All rights reserved.

1. Introduction

Hydrogen is a clean renewable energy source and has been pursued as one of the promising alternatives to fossil fuels due to increasing global energy demands and climate change [1,2].

* Corresponding author.

E-mail address: liuzq_hgxy@scu.edu.cn (Z. Liu).

Splitting water via electrochemical reactions is considered to be the most promising approach towards hydrogen production. Efficient water splitting requires high active electrocatalysts to lower the overpotentials of the hydrogen evolution reaction (HER) at the cathode and the oxygen evolution reaction (OER) at the anode, eventually in order to facilitate the hydrogen production [3]. Precious metals (Pt, Pd, Ir, Ru, etc.) provide an excellent electrocatalytic surface that demonstrates low overpotentials, exemplified by an anodic electrocatalyst with the formula $\text{Ir}_x\text{Ru}_y\text{Ta}_z\text{O}_2$ registering an electric consumption of $42 \text{ kW h kg}^{-1}\text{H}_2$ and an energy efficiency of 94% [4]. However, the high cost and scarcity of the precious metals hinder the application in industry. Thus, it is highly expected to develop non-precious metal catalysts that can utilize low value energy such as the low-temperature waste heat under the premise of both low materials cost and reduced energy input.

A narrow band gap II–VI semiconductor, PbTe has an fcc cubic crystallographic structure with a lattice constant of 0.646 nm, constituted of Pb^{2+} and Te^{2-} connected by metallic bonds. PbTe semiconductors are well known for their symmetric energy band structure, a narrow band gap of 0.31 eV, a large Bohr exciton radius of 46 nm, good conductivity of $28.29\text{--}99.50 \text{ S cm}^{-1}$, and large electron and hole transport rates of 1730 and $780 \text{ cm}^2 \text{ V}^{-1} \text{ s}^{-1}$. PbTe semiconductors are regarded highly promising in applications such as thermoelectric conversion [5], far infrared detection (3–30 μm) [6], and photoelectro-chemical devices [7]. More recently, a novel system that may greatly expand the application of PbTe semiconductors has been proposed [8]. This design can generate a novel pathway to produce chemical energy from low quality waste heat. In the study, we prepared PbTe-PbS/ TiO_2 nanotube arrays (PbTe-PbS/TNAs) by using the successive ionic layer adsorption and reaction (SILAR) followed by linear sweep voltammetry (LSV). At 70 °C and cell voltage of 1.0 V, the system registered an energy efficiency of 88.5% and a heat efficiency of 49.9%. Ordered mesoporous carbon (OMC), since its discovery in 1999 [9], has attracted a great deal of attention owing to its distinguished properties of extremely well-ordered pore structure, high specific pore volume, high specific surface area, large adsorption capacities, low electron-transfer resistance, and chemical inertness. These advantages make it suitable for applications in adsorption [10], chemical sensors [11], catalyst carriers [12], energy storage [13] and new functional composite materials [14]. As reported, OMC CMK-3 offered faster electron-transfer kinetics than glassy carbon, fullerenes, or even CNTs, resulting in increasing the intensity of voltammetric peaks and lowering the overpotentials [15]. The OMC modified glass carbon electrode (OMCs/GCE) can remarkably enhance electrocatalytic activity towards the oxidation of ractopamine with a great increase of peak current [16], and reduce the oxidation overpotential and improve the current response of phenols to some extent [17]. Because of the good absorptivity, conductivity, electron restorage/releasing capacity of OMC, this family of materials can effectively improve the adsorption and reaction of chemical species inside the mesopores, enhance the charge transfer efficiency of the key reaction elemental steps, thus greatly increasing reaction rates. To further promote the catalytic reaction kinetics and improve the energy efficiency in the current work, we apply OMC as the charge transport layer and electrochemical reaction interface of the PbTe-PbS/TNAs electrode, and drive the anodic reaction ($\text{SO}_3^{2-} + \text{S}^{2-} \rightarrow \text{S}_2\text{O}_3^{2-} + 2\text{e}^-$) proceeding both at the OMC surface and the PbTe-PbS nanocrystal surface. The results show that OMC modification can reduce the resistance of the electrode process, improve the energy band bending of the electrode/electrolyte interface, increase the active electrochemical surface area of the electrode, enhance the charge transfer between the electrode surface and the electrolyte solution and charge transport

within the OMC phases, decrease the polarization of the electrode, as well as enhance short circuit current density upon increasing temperature of PbTe/PbS/TNAs electrode. The overall results are the enhanced electrocatalytic activities towards hydrogen production.

2. Experimental

2.1. OMC/PbTe-PbS/TNAs preparation

The preparation method and procedure details of PbTe-PbS/TNAs can be found in our published work [18,19]. The OMC was first dealt with hydrophilic pretreatment prior to deposition. 0.1 g CMK-3 was added to H_2O_2 (10%), stirred at 60 °C for 2 h. After cooled to room temperature, the sample was centrifugated three times and decanted of the supernatant. The solid was placed in an oven (60 °C) before following experimental procedures. 5.0 mg hydrophilic OMC was added to 100 μL Nafion solution (5%) mixed in 1 mL ethanol, and ultrasonicated for 30 min to obtain the OMC/Nafion dispersion. The dispersion was applied to the PbTe-PbS/TNAs electrode by using a micro-syringe with an amount of 5–15 $\mu\text{L cm}^{-2}$. The electrode was then dried at 60 °C for 2 h and labeled OMC/PbTe-PbS/TNAs. For comparison, a PbTe-PbS/TNAs electrode was modified with Nafion only and labeled Nafion/PbTe-PbS/TNAs, and a PbTe/TNAs electrode modified with OMC/Nafion without the linear sweep voltammetry sulfuration was labeled OMC/PbTe/TNAs.

2.2. Characterization method

X-ray diffraction (XRD) analysis was carried out on a Philips XPert pro MPD to investigate the crystalline phases of the samples. Scanning electron microscopy (SEM) was performed on a JSM-7500F to provide the surface morphology and chemical composition of the samples. Fourier transform infrared spectrophotometry was applied on a Nicolet 6700 spectrometer to examine the functional groups and contents of the samples. Raman spectrometry was conducted on a LabRAM HR spectrometer to analyze the sample surfaces.

2.3. Electrochemical measurements

A CHI660E electrochemical work station was used for all electrochemical measurements, including linear sweep voltammetry (LSV), electrochemical impedance spectroscopy (EIS), Tafel curves, Mott-Schottky curves. The three electrode system was constituted of a sample working electrode, a platinum counter electrode, and an SCE reference electrode. The electrolyte was $0.5 \text{ mol L}^{-1} \text{ Na}_2\text{SO}_3 + 0.5 \text{ mol L}^{-1} \text{ Na}_2\text{S}$ solution. During LSV, the starting and ending voltages were -0.5 V and $+0.5 \text{ V}$, respectively, with a scanning rate of 10 mV s^{-1} . The EIS measurement was conducted at a voltage of the open circuit voltage of each sample in the frequency range of $0.01\text{--}10^5 \text{ Hz}$. The Tafel analysis was performed in the potential range of open circuit voltage $\pm 0.15 \text{ V}$ with a scanning rate of 0.05 mV s^{-1} . Unless specified, all electrochemical measurements were carried out at 25 °C.

2.4. Electrochemical hydrogen production

The hydrogen production experiments were carried out at a direct current potentiostat in a two-electrode cell. The sample was the anode and a Pt foil the cathode, with an inter-electrode distance of 10 cm under cell voltages from 1.0 V to 1.5 V at a fixed temperature of 55 °C. The other conditions were the same as the LSV test. The volume of produced H_2 gas was measured via water

expulsion with a specifically scaled upside-down funnel. Electricity consumption, energy efficiency and heat efficiency were estimated referring to our previous method [8].

3. Results and discussion

Fig. 1 depicts the small-angle XRD patterns (a), FTIR spectra (b) and Raman spectra (c) of the OMC before and after treatment with H_2O_2 . From Fig. 1(a), both the pristine OMC and the OMC treated with H_2O_2 show a 2θ peak ca. 1° which stands for diffraction peak (100) of 2D hexagonal structure ($P6mm$), indicating an ordered mesoporous structure [20,21]. Compared to the OMC, the diffraction peak (100) of the OMC treated with H_2O_2 shifts to a smaller angle and is strengthened to some extent, suggesting that the mesoporous size should be enlarged and the pore order degree is enhanced. In Fig. 1(b), absorption bands at 3438, 1576, and 1137 cm^{-1} are ascribed to the symmetric vibrations of $-\text{OH}$, $\text{C}=\text{O}$, and $\text{C}-\text{O}$ [20,22]. The symmetric vibration of $-\text{OH}$ was enhanced obviously after H_2O_2 treatment, implying improved hydrophilicity of OMC which was originally hydrophobic. In Raman spectra shown in Fig. 1(c), both the spectra of the OMC before and after treatment with H_2O_2 showed the presence of D and G bands, located at 1320 cm^{-1} (disorder mode) and 1585 cm^{-1} (tangential), which are ascribed to the defects/imperfections and hexagonal graphene plane, respectively [23,24]. The I_D/I_G of the OMC pretreated with H_2O_2 was slightly lower than that of the OMC, indicating that defects and imperfections were reduced at some extent [25]. These results imply that the H_2O_2 pretreatment of OMC was beneficial to the mass transfer and electron exchange in the electrochemical reactions. The wide-angle XRD patterns of the samples are shown

in Fig. S1. It can be seen that for the PbTe/TNAs, the diffraction peaks of (111), (200), {220}, (222), (400), (420) and (422) are well-resolved (JCPDS#65-0470), which correspond to face-centred cubic PbTe [7,26]. For the PbTe-PbS/TNAs, besides these peaks, the new peaks of {200}, {220}, {400}, {331} ascribed to PbS phases (JCPDS#05-0692) are unveiled [27], and the obviously reduced peaks assigned to PbTe phases are attributed to the covering of PbTe surface by PbS, which resulted from in situ substitution of sulfur for tellurium due to lower formation enthalpy of PbS ($-98.74\text{ kJ mol}^{-1}$) than that of PbTe ($-69.50\text{ kJ mol}^{-1}$) ($\text{PbTe} + \text{S}^{2-} \rightarrow \text{PbS} + \text{Te}^{2-}$) [8]. Fig. S2 presents the representative SEM images of the PbTe-PbS/TNAs, illustrating a large quantity of PbTe-PbS nanoparticles deposited on the surface of TiO_2 arrays, and the inner and outer walls of TiO_2 tubes while the tube openings were not clogged with the nanoparticles. Fig. 2 shows the elemental mapping of OMC/PbTe-PbS/TNAs. It can be seen that the sample contained Ti, O, Pb, Te, S, and C. Ti and O covered the whole sample region, while Te, S, and Pb took up the same regions. A closer look shows that the Pb distribution occupied the Te and S regions, and corresponded with the Ti and O regions. The explanation is that PbTe-PbS deposition took place on top of TiO_2 , while Te and S combined with Pb. From Table S1, the EDS diagrams of the samples reveal that the atomic ratios of Te and S versus Pb in PbTe-PbS/TNAs and OMC/PbTe-PbS/TNAs were 1.21 and 1.33, respectively, both greater than 1.0. The discrepancy is attributed to that besides PbTe, the Te components in the samples also existed in the forms of TeO_2 and Na_2Te .

Fig. 3 shows the LSV curves of OMC/PbTe-PbS/TNAs prepared with OMC/Nafion of $5\text{--}25\text{ }\mu\text{L cm}^{-2}$. When the amount of OMC/Nafion was increased from $5\text{ }\mu\text{L cm}^{-2}$ to $15\text{ }\mu\text{L cm}^{-2}$, the

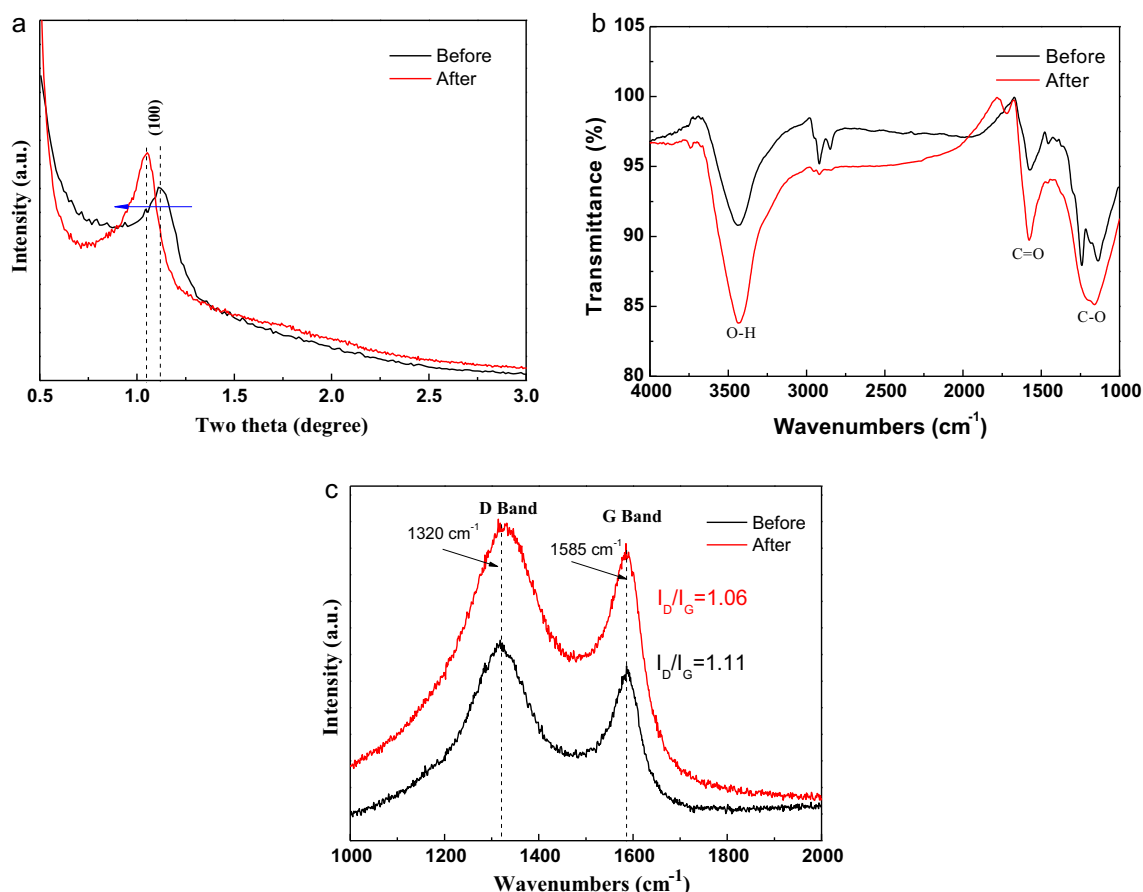


Fig. 1. Small-angle XRD patterns (a), FTIR spectra (b) and Raman spectra (c) of the OMC before and after treatment with H_2O_2 .

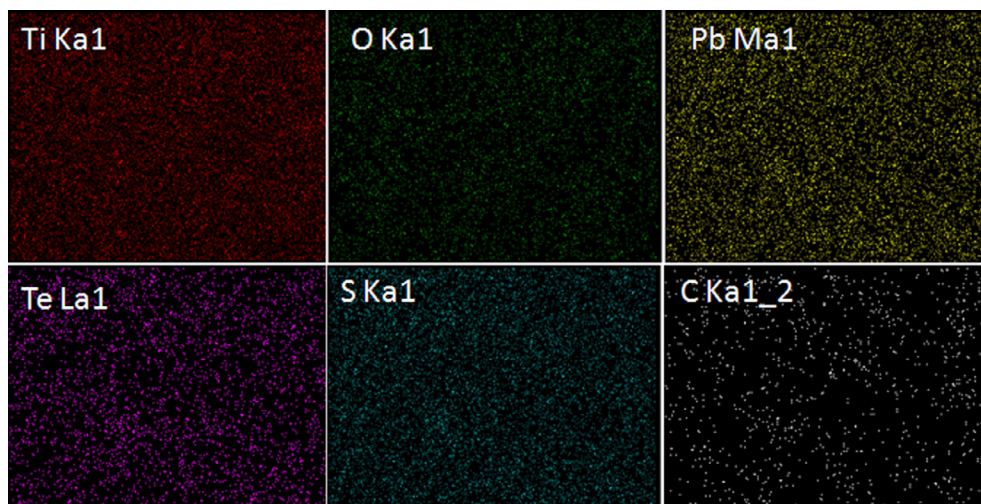


Fig. 2. Elemental mapping of the OMC/PbTe-PbS/TNAs.

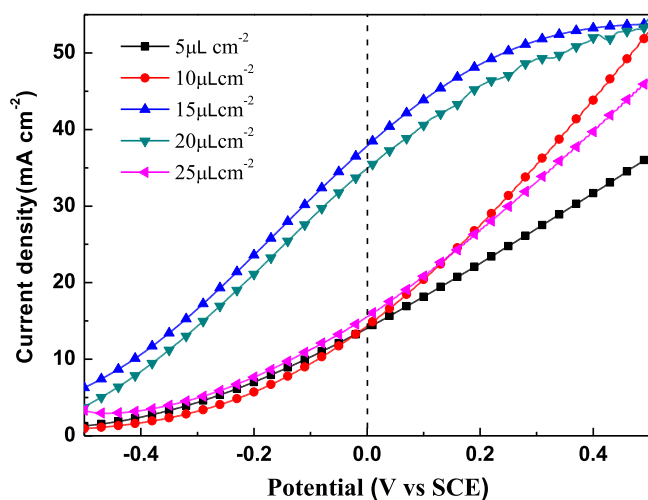


Fig. 3. Current-voltage characteristics of the PbTe-PbS/TNAs modified with various OMC dosages at 25 °C.

current response increased. When the amount of OMC/Nafion was greater than $15 \mu\text{L cm}^{-2}$, the current response decreased. The results demonstrate that for the PbTe-PbS/TNAs electrode, $15 \mu\text{L cm}^{-2}$ of OMC/Nafion was the optimum amount. When the OMC/Nafion amount was smaller than this value, OMC acted as the charge carrier to benefit the electron transfer and the adsorption of electrolyte by the electrode was the major process. When the OMC/Nafion amount was greater than the optimum value, the increased thickness hindered the diffusion of electrolyte towards the TNAs inside portions and delayed the electron transfer to TNAs. To distinguish whether OMC or Nafion contributed to the electrochemical property variation, we modified TNAs, PbTe-PbS/TNAs and PbTe/TNAs with either OMC or Nafion, labeled with OMC or Nafion, both at $15 \mu\text{L cm}^{-2}$. The current-voltage characteristics of OMC/TNAs, Nafion/PbTe-PbS/TNAs, OMC/PbTe-PbS/TNAs, and OMC/PbTe/TNAs electrodes are compared to that of PbTe-PbS/TNAs, Fig. 4. According to the figure, the short circuit current density of OMC/TNAs was very weak, at only $0.00952 \text{ mA cm}^{-2}$, close to that of TNAs. The result means that either OMC or Nafion did not contribute significantly to the electrode activity. When only Nafion was used to modify PbTe-PbS/TNAs, the short circuit current density decreased from

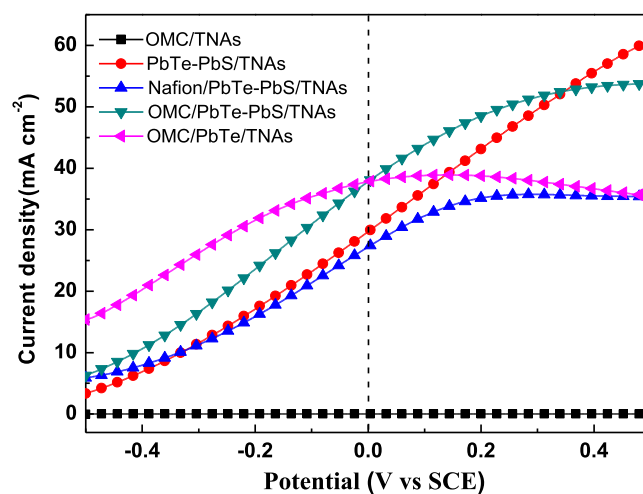


Fig. 4. Current-voltage characteristics of the samples at 25 °C.

29.68 mA cm^{-2} to 27.2 mA cm^{-2} . This is because Nafion is not electrically active with poor conductivity. The electrostatic attraction moved external redox species into the Nafion membrane as the conducting ions. The charge transfer inside the membrane relied on the diffusion of ions or electroactive species, and the migration of the neighbouring redox centers. And then charge transfer went on from poor conductive Nafion to PbTe-PbS/TNAs. Therefore, when only Nafion was used to modify the electrodes, the charge transfer in electrochemical reactions was damped. When OMC/Nafion was used to modify PbTe-PbS/TNAs, the current density was increased with a short circuit current density of 37.84 mA cm^{-2} , a 27.49% increase over that of PbTe-PbS/TNAs (29.68 mA cm^{-2}). Although the short circuit current density of OMC/PbTe/TNAs was almost the same as that of OMC/PbTe-PbS/TNAs, the current density of OMC/PbTe/TNAs did not increase when the bias voltage was further augmented. For OMC/PbTe-PbS/TNAs at a bias voltage of $+0.5 \text{ V}$, the current density reached the peak value. The above LSV results illustrate that the formation of PbS shell over PbTe/TNAs increased the effective charge carrier density inside the electrode. The charge carriers inside the PbTe-PbS/TNAs included both the heat excited electrons by the *n*-type PbTe donor energy level, and the heat induced holes by the *p*-type PbS acceptor energy level [8]. In the mean time, OMC

and Nafion themselves were not electroactive species. Because of their great specific surface areas, good conductivity and electron restorage and releasing capacity, these species augmented the electrochemical reactions at the electrode surface and the charge transfer between the electrode surface and the electrolyte.

Electrochemical impedance spectrometry (EIS) was conducted on PbTe-PbS/TNA, Nafion/PbTe-PbS/TNAs, and OMC/PbTe-PbS/TNAs, Fig. 5. The Nyquist equivalent circuit is shown in Fig. 5(a) as the inset. R_s is the electrolyte resistance, R_1 and C_1 are the charge transport resistance and capacity inside the electrode, R_2 and C_2 are the charge transport resistance and double layer capacity at the interface between the electrode and electrolyte, and R_w is the Warburg impedance of the electrode process [28,29]. The existence of R_w indicates concentration polarization during the electrode process, whose value represents the effect of the electrode surface diffusion process on the charge carrier transport consumption. According to the simulated data of the equivalent circuit presented in Table S2, for PbTe-PbS/TNAs, Nafion/PbTe-PbS/TNAs, and OMC/PbTe-PbS/TNAs, R_2 values are greater than R_1 values by one order of magnitude. Combined with the existence of R_w , it is speculated that the charge transfer between the electrode surface and electrolyte could be the limiting step of the electrode process. Among the three samples, OMC/PbTe-PbS/TNAs had the smallest R_2 , indicating the OMC/Nafion modification strengthened the charge transfer between the electrode surface and electrolyte. Accordingly, Nafion/PbTe-PbS/TNAs had the largest R_2 and a much greater time constant $\tau_2 = R_2 \times C_2$ (In Fig. 5(b)) than OMC/PbTe-PbS/TNAs and PbTe-PbS/TNAs, illustrating modification with Nafion alone would hinder the effective wetness of the electrode surface by electrolyte, and reduce the electron transfer rate between the electrode surface and electrolyte [30].

Electrode polarization is caused by extended exchange current density. A large exchange current density induces a small driving force required by an electrode reaction. In contrast, a small exchange current density indicates a great driving force required by an electrode reaction [31,32]. In the Tafel curve in Fig. 6(a), the current density at zero overpotential represents the exchange current density of the samples. It is clear that the exchange current densities of PbTe-PbS/TNAs, Nafion/PbTe-PbS/TNAs, and OMC/PbTe-PbS/TNAs are very close to each other. This means modification with Nafion and/or OMC did not change the reversibility and level of difficulty of the electrode reactions. When the overpotential was greater than zero, the right side Tafel curve being the anodic polarization curve, the polarization current densities followed the order at the same overpotential: OMC/PbTe-PbS/TNAs > Nafion/PbTe-PbS/TNAs > PbTe-PbS/TNAs. The results demonstrate that modification with Nafion and/or OMC had a positive effect on strengthening the electrode process, while

the best electrode property was obtained under modification with OMC/Nafion. Fig. 6(b) shows the Mott-Schottky curves of the samples. In the figure, the slopes of the three curves are all positive, suggesting that modification with Nafion and/or OMC did not change the charge carrier type of the electrodes, n -type semiconductor. The tangents of the linear portion of the Mott-Schottky curves represent the flat band potential of the electrode E_{FB} , and the degree of slopes corresponds to the level of the electrode surface charge density [33]. The order of sample flat band potentials is OMC/PbTe-PbS/TNAs > PbTe-PbS/TNAs > Nafion/PbTe-PbS/TNAs, while the order of the slopes has the reverse direction. The phenomenon shows that modification with Nafion and/or OMC changed the electrode surface charge density and the redox potential. Modification with OMC/Nafion enhanced the energy band bending degree of the electrolyte and electrode surface, strengthened the charge transfer between the electrode and electrolyte, reduced the accumulation of electrode surface charges, decreased the polarization degree of the electrode progress, and accelerated the electrode process. We also estimated the relative differences in the electrochemically active surface area (ECSA) using a simple cyclic voltammetry (CV) method [34]. The current response in the potential window used for CV (-0.893 to -0.693 V vs. SCE) at different scan rates (40 – 280 mV s^{-1}) should be mostly due to the charging of the double-layer (Fig. 7(a)–(c)). The double layer capacitances (C_{dl}) for each sample, which should be directly proportional to the surface area, were extracted by plotting $\Delta j = j_a - j_c$ at a given potential (-0.793 V vs. SCE) against the CV scan rates (Fig. 7(d)) [35,36]. The proliferation of active sites illustrated that C_{dl} for OMC/PbTe-PbS/TNAs (29 mF cm^{-2}) is about 1.37 and 2.59 times larger as compared to that for Nafion/PbTe-PbS/TNAs and PbTe-PbS/TNAs, respectively. This increase in the ECSA demonstrates the proliferation of the active sites, which certainly indicates that OMC contributed to a large functioning surface area, and thus improved electrocatalytic performance, well in agreement with the results of antecedent electrochemical analyses.

Fig. 8 shows the linear voltage-current characteristic curves, electrochemical impedance spectrometric curves and Tafel curves of OMC/PbTe-PbS/TNAs at different temperatures. With increasing electrolyte temperature, Fig. 8(a) displays that current density increased with a short circuit current density of 130.6 mA cm^{-2} at 65°C , 3.45 times the value of 37.84 mA cm^{-2} at 25°C ; Fig. 8(b) reveals the radius of the Nyquist arcs decreased; and Fig. 8(c) shows the current density increased slightly at the overpotential of zero, with an exchange current density of 0.197 mA cm^{-2} at 65°C , a 29.61% increase over that of 0.152 mA cm^{-2} at 25°C . The Tafel curve slope decreases with increasing electrolyte temperature. These results demonstrate the OMC/PbTe-PbS/TNAs electrode inherited the excellent hot electron extraction capability of the

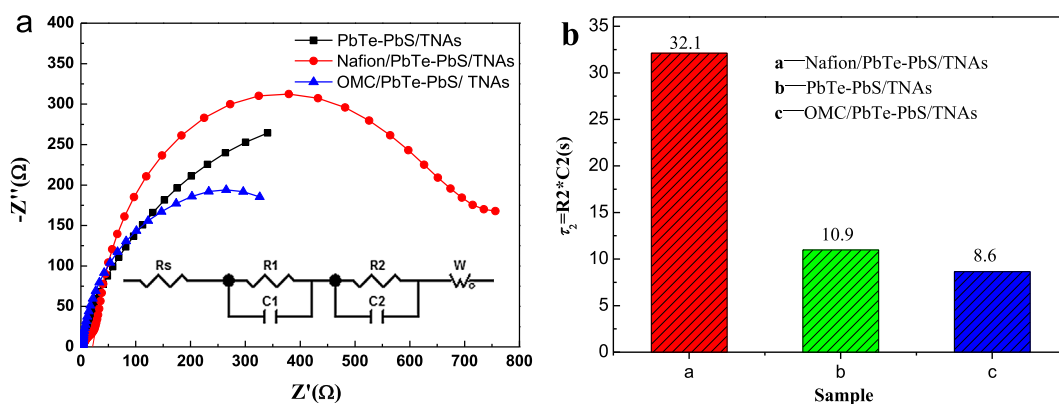


Fig. 5. Nyquist plots (a) and corresponding time constant histogram (b) of the samples at 25°C . The inset is the equivalent circuit in Nyquist plots.

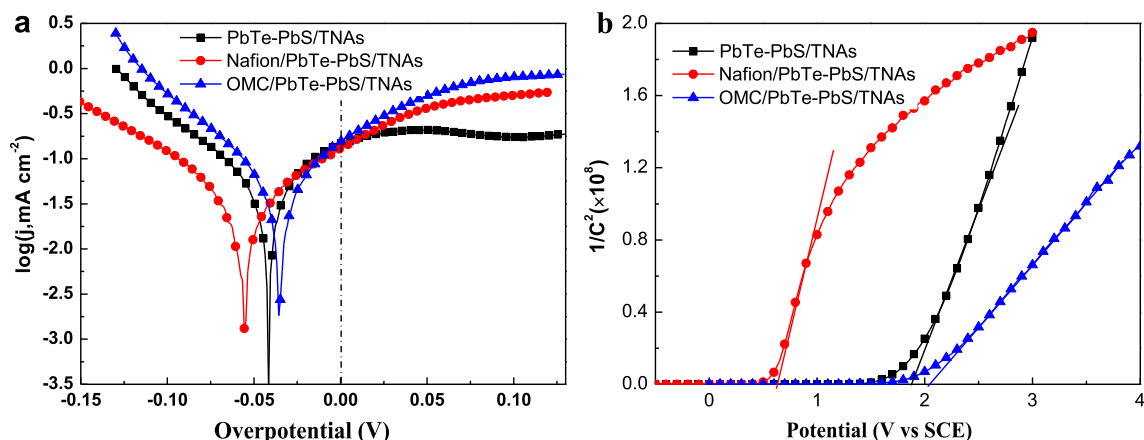


Fig. 6. Tafel plots (a) and Mott-Schottky curves (b) of the samples at 25 °C.

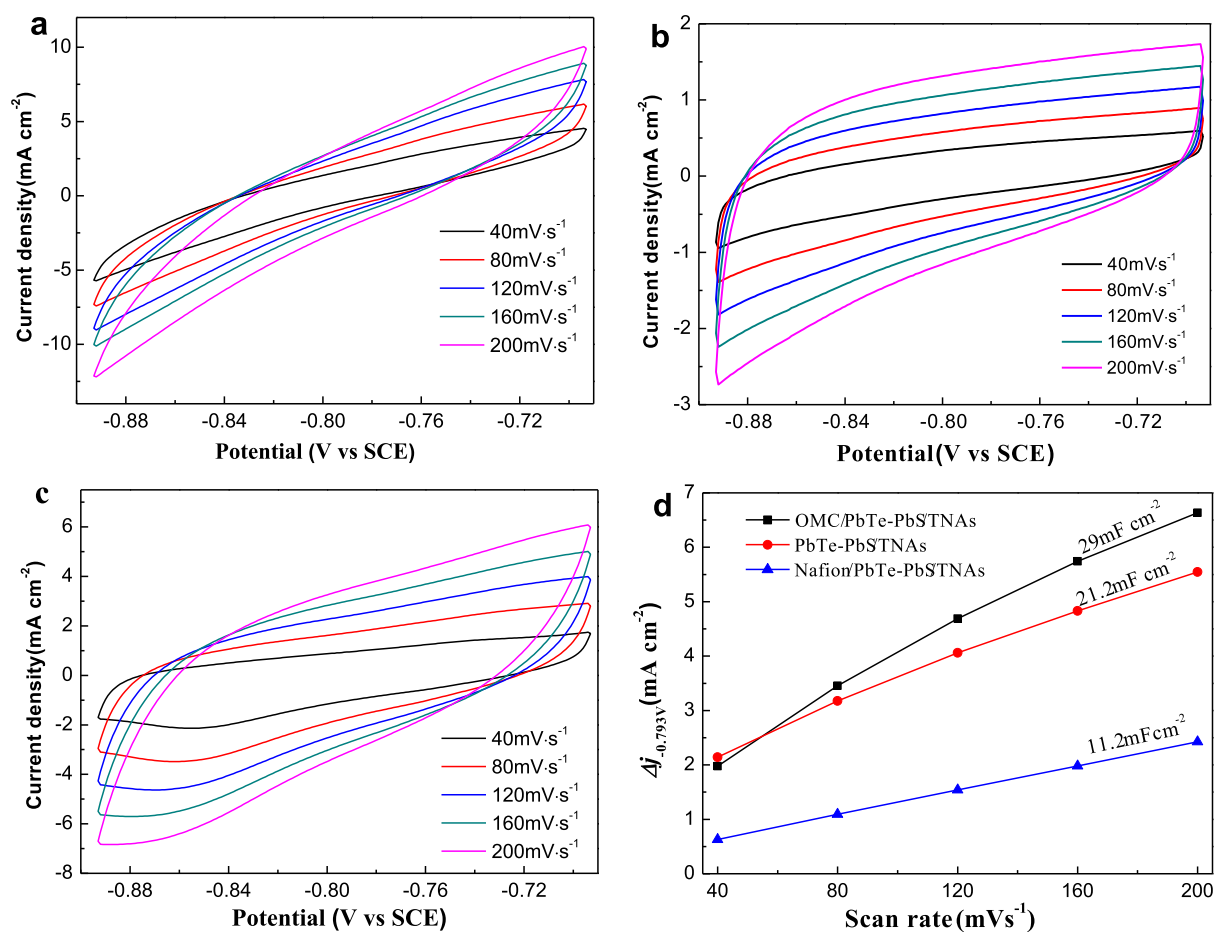


Fig. 7. Cyclic voltammograms of the (a) PbTe-PbS/TNAs, (b) Nafion/PbTe-PbS/TNAs and (c) OMC/PbTe-PbS/TNAs at various scan rates (40–200 mV s⁻¹) used to (d) estimate the C_{dl} and relative electrochemically active surface area.

PbTe-PbS/TNAs electrode, and its electrode process increased rapidly with higher temperature.

The electricity consumption, energy efficiency and heat efficiency were calculated from the data from hydrogen production experiments referring to our previous method [8], as shown in Fig. 9. It can be seen that with increasing cell voltage, the hydrogen production rate and electricity consumption increased rapidly, whereas the energy efficiency decreased slightly and

heat efficiency was stable at about 43%. Significantly, the hydrogen production rate and energy efficiency were obviously higher than that of PbTe-PbS/TNAs electrode at similar conditions, strongly supporting electrochemical analyses. Under bath voltage of 1.0 V at 55 °C, the OMC/PbTe-PbS/TNAs electrode presented a hydrogen production rate of 11 mL cm⁻² h⁻¹ and an energy efficiency of 98.79%, consuming electric power of 26.84 kW h kg⁻¹ H₂.

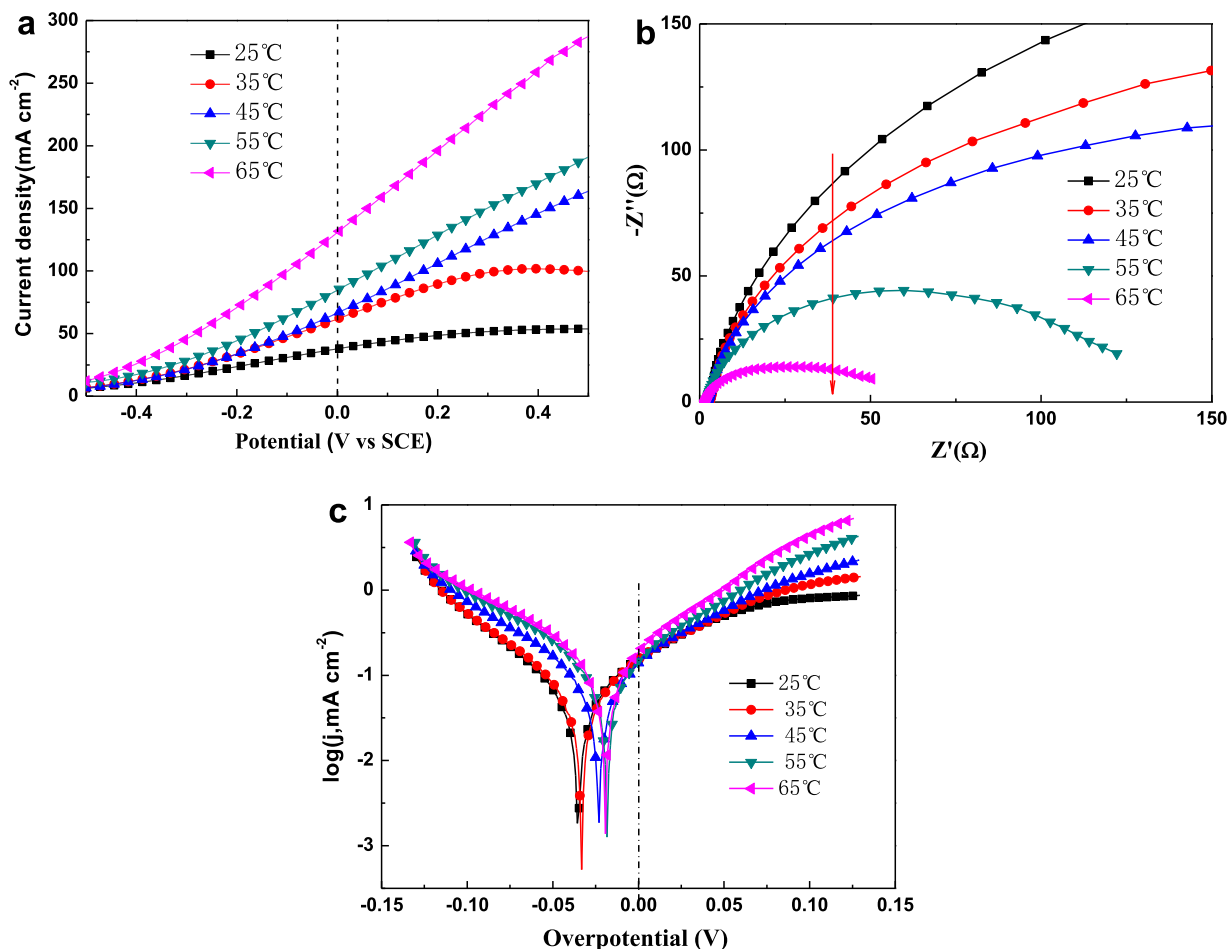


Fig. 8. Current-voltage characteristics (a), Electrochemical impedance spectra (b) and Tafel plots (c) of the OMC/PbTe-PbS/TNAs at various temperatures.

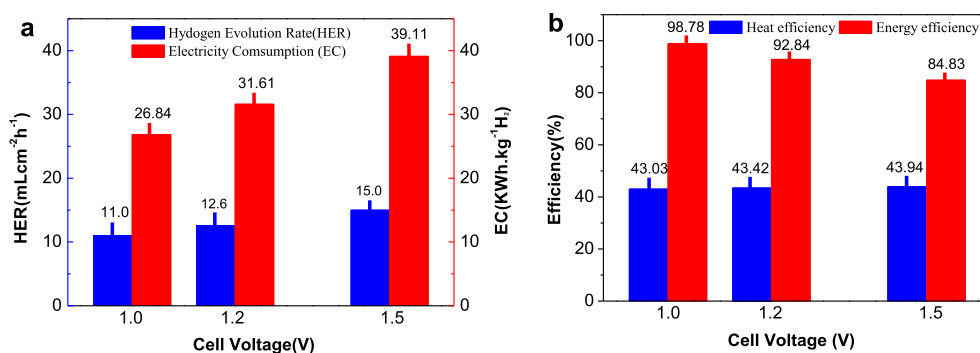


Fig. 9. Hydrogen evolution rate and electricity consumption (a), and heat efficiency and energy efficiency (b) for the two electrode system of OMC/PbTe-PbS/TNAs as an anode under various cell voltages at 55 °C.

4. Conclusions

Modification of PbTe-PbS/TNAs, TNAs, and PbTe/TNAs electrodes with OMC and/or Nafion provided OMC/PbTe-PbS/TNAs, Nafion/PbTe-PbS/TNAs, OMC/TNAs, and OMC/PbTe/TNAs electrodes, and the microscopic structure and electrochemical properties of the modified electrodes were investigated. Modification of PbTe-PbS/TNAs with OMC and Nafion could improve the energy band bending of the electrode/electrolyte interface, increase the active electrochemical surface area of the electrode, reduce the

electrode process resistance, and strengthen the electrode process. The hot electron extraction capability of the PbTe-PbS/TNAs electrode remained in the OMC/Nafion modified sample to provide a rapid enhancement of short circuit current density upon increasing temperature. The electrochemical impedance and Tafel slope decreased accordingly, leading to accelerated electrode process upon increased temperature. The OMC/PbTe-PbS/TNAs electrode provided a hydrogen production rate of 11 mL cm⁻² h⁻¹ and an energy efficiency of 98.79% under bath voltage of 1.0 V at 55 °C.

Acknowledgements

This work was supported by the National Science Foundation of China – China (Grant No. 21376154). The authors would like to express their heartfelt gratitude to Analytical and Test Center of Sichuan University.

Appendix A. Supplementary data

Supplementary data associated with this article can be found, in the online version, at <http://dx.doi.org/10.1016/j.jcis.2017.06.015>.

References

- [1] S. Chu, A. Majumdar, Opportunities and challenges for a sustainable energy future, *Nature* 488 (2012) 294–303.
- [2] M.G. Walter, E.L. Warren, J.R. McKone, S.W. Boettcher, Q. Mi, E.A. Santori, N.S. Lewis, Solar water splitting cells, *Chem. Rev.* 110 (2010) 6446–6473.
- [3] N. Jiang, B. You, M. Sheng, Y. Sun, Electrodeposited cobalt-phosphorous-derived films as competent bifunctional catalysts for overall water splitting, *Angew. Chem. Int. Ed.* 54 (2015) 6251–6254.
- [4] A.T. Marshall, S. Sunde, M. Tsypkin, R. Tunold, Performance of a PEM water electrolysis cell using $\text{Ir}_x\text{Ru}_y\text{Ta}_z\text{O}_2$ electrocatalysts for the oxygen evolution electrode, *Int. J. Hydrogen Energy* 32 (2007) 2320–2324.
- [5] M. Ibáñez, R. Zamani, S. Gorsse, J. Fan, S. Ortega, D. Cadavid, J.R. Morante, J. Arbiol, A. Cabot, Core-shell nanoparticles as building blocks for the bottom-up production of functional nano composites: PbTe-PbS thermoelectric properties, *ACS Nano* 7 (2013) 2573–2586.
- [6] Z. Han, V. Singh, D. Kita, C. Monmeyran, P. Becla, P. Su, J. Li, X. Huang, L.C. Kimerling, J. Hu, K. Richardson, D.T.H. Tan, A. Agarwal, On-chip chalcogenide glass waveguide-integrated mid-infrared PbTe detectors, *Appl. Phys. Lett.* 109 (2016) 07111.
- [7] J.E. Murphy, M.C. Beard, A.G. Norman, S.P. Ahrenkiel, J.C. Johnson, P. Yu, O.I. Micic, R.J. Ellingson, A.J. Nozik, PbTe colloidal nanocrystals: synthesis, characterization, and multiple exciton generation, *J. Am. Chem. Soc.* 128 (2006) 3241–3247.
- [8] Z.Q. Liu, X.H. Cao, B. Wang, M. Xia, S. Lin, Z.H. Guo, X.M. Zhang, S.Y. Gao, Coupling thermoelectricity and electrocatalysis for hydrogen production via PbTe-PbS/TiO₂ heterojunction, *J. Power Sources* 342 (2017) 452–459.
- [9] R. Ryoo, S.H. Joo, S. Jun, Synthesis of highly ordered carbon molecular sieves via template-mediated structural transformation, *J. Phys. Chem. B* 103 (1999) 7743–7746.
- [10] K. Kwon, Y.J. Sa, J.Y. Cheon, S.H. Joo, Ordered mesoporous carbon nitrides with graphitic frameworks as metal-free, highly durable, methanol-tolerant oxygen reduction catalysts in an acidic medium, *Langmuir* 28 (2012) 991–996.
- [11] M. Zhou, J. Ding, L.P. Guo, Q.K. Shang, Electrochemical behavior of L-cysteine and its detection at ordered mesoporous carbon-modified glassy carbon electrode, *Anal. Chem.* 79 (2007) 5328–5335.
- [12] D.S. Yang, D. Bhattacharjya, S. Inamdar, J. Park, J.S. Yu, Phosphorus-doped ordered mesoporous carbons with different lengths as efficient metal-free electrocatalysts for oxygen reduction reaction in alkaline media, *J. Am. Chem. Soc.* 134 (2012) 16127–16130.
- [13] Y. Mao, H. Duan, B. Xu, L. Zhang, Y.S. Hu, C.C. Zhao, Z.X. Wang, L.Q. Chen, Y.S. Yang, Lithium storage in nitrogen-rich mesoporous carbon materials, *Energy Environ. Sci.* 5 (2012) 7950–7955.
- [14] G. Yue, J. Wu, Y. Xiao, M. Huang, J. Lin, J.Y. Lin, High performance platinum-free counter electrode of molybdenum sulfide-carbon used in dye-sensitized solar cells, *J. Mater. Chem. A* 1 (2013) 1495–1501.
- [15] M. Zhou, J. Guo, L. Guo, J. Bai, Electrochemical sensing platform based on the highly ordered mesoporous carbon-fullerene system, *Anal. Chem.* 80 (2008) 4642–4650.
- [16] X. Yang, B. Feng, P. Yang, Y. Ding, Y. Chen, J. Fei, Electrochemical determination of toxic ractopamine at an ordered mesoporous carbon modified electrode, *Food Chem.* 145 (2014) 619–624.
- [17] J.C. Ndamaniha, L. Guo, Ordered mesoporous carbon for electrochemical sensing: a review, *Anal. Chim. Acta* 747 (2012) 19–28.
- [18] X. Liu, Z.Q. Liu, J. Lu, X.L. Wu, W. Chu, Silver sulfide nanoparticles sensitized titanium dioxide nanotube arrays synthesized by in situ sulfurization for photocatalytic hydrogen production, *J. Colloid Interface Sci.* 413 (2014) 17–23.
- [19] X.M. Zhang, B. Wang, Z.Q. Liu, Tuning PbS QDs deposited onto TiO₂ nanotube arrays to improve photoelectrochemical performances, *J. Colloid Interface Sci.* 484 (2016) 213–219.
- [20] N. Liu, L. Yin, C. Wang, L. Zhang, N. Lun, Dong Xiang, Y. Qi, R. Gao, Adjusting the texture and nitrogen content of ordered mesoporous nitrogen-doped carbon materials prepared using SBA-15 silica as a template, *Carbon* 48 (2010) 3579–3591.
- [21] A. Nsabimana, X. Bo, Y. Zhang, M. Li, C. Han, L. Guo, Electrochemical properties of boron-doped ordered mesoporous carbon as electrocatalyst and Pt catalyst support, *J. Colloid Interface Sci.* 428 (2014) 133–140.
- [22] J.L. Figueiredo, M.F.R. Pereira, M.M.A. Freitas, J.J.M. Orfao, Modification of the surface chemistry of activated carbons, *Carbon* 37 (1999) 1379–1389.
- [23] S. Bhattacharyya, C. Cardinaud, G. Turban, Spectroscopic determination of the structure of amorphous nitrogenated carbon films, *J. Appl. Phys.* 83 (1998) 4491–4500.
- [24] N. Jia, Z. Wang, G. Yang, H. Shen, L. Zhu, Electrochemical properties of ordered mesoporous carbon and its electroanalytical application for selective determination of dopamine, *Electrochem. Commun.* 9 (2007) 233–238.
- [25] R. Jin, G. Chen, J. Pei, C. Yan, Hydrothermal synthesis and thermoelectric transport property of PbS–PbTe core-shell heterostructures, *New J. Chem.* 36 (2012) 2574–2579.
- [26] Q. Kang, S. Liu, L. Yang, Q. Cai, C.A. Grimes, Fabrication of PbS nanoparticle sensitized TiO₂ nanotube arrays and their photoelectrochemical properties, *ACS Appl. Mater. Interfaces* 3 (2011) 746–749.
- [27] Q. Dong, W. Liao, B. Wang, Z.Q. Liu, Investigation of interfacial and photoelectrochemical characteristics of thermally treated PbS/TiO₂ photoanodes, *RSC Adv.* 5 (2015) 33869–33877.
- [28] X.S. Li, Z.Y. Zhang, G.M. Bai, C.X. Du, C.F. Ma, A photoelectrochemical investigation of the hydrogen-evolving doped TiO₂ nanotube arrays electrode, *Int. J. Hydrogen Energy* 37 (2012) 854–859.
- [29] Z.Q. Liu, B. Wang, J.C. Wu, Q. Dong, X.M. Zhang, H. Xu, Effects of hydroxylation on PbS quantum dot sensitized TiO₂ nanotube array photoelectrodes, *Electrochim. Acta* 187 (2016) 480–487.
- [30] K.C. Pham, Y.H. Chang, D.S. McPhail, G. Mattevi, A. T. S. Wee, D. H. C. Chua, Amorphous molybdenum sulfide on graphene-carbon nanotube hybrids as highly active hydrogen evolution reaction catalysts, *ACS Appl. Mater. Interfaces* 8 (2016) 5961–5971.
- [31] J. Kibsgaard, T.F. Jaramillo, Molybdenum Phosphosulfide: An active, acid-stable, earth-abundant catalyst for the hydrogen evolution reaction, *Angew. Chem. Int. Ed.* 53 (2014) 14433–14437.
- [32] E.J. Popczun, J.R. McKone, C.G. Read, A.J. Biacchi, A.M. Wiltrout, N.S. Lewis, R.E. Schaak, Nanostructured nickel phosphide as an electrocatalyst for the hydrogen evolution reaction, *J. Am. Chem. Soc.* 135 (2013) 9267–9270.
- [33] A. Wolcott, W.A. Smith, T.R. Kuykendall, Y.P. Zhao, J.Z. Zhang, Photoelectrochemical water splitting using dense and aligned TiO₂ nanorod arrays, *Small* 5 (2009) 104–111.
- [34] E.J. Popczun, C.G. Read, C.W. Roske, N.S. Lewis, R.E. Schaak, Highly active electrocatalysis of the hydrogen evolution reaction by cobalt phosphide nanoparticles, *Angew. Chem. Int. Ed.* 53 (2014) 5427–5430.
- [35] M.A. Lukowski, A.S. Daniel, C.R. English, F. Meng, A. Forticaux, R.J. Hamers, S. Jin, Highly active hydrogen evolution catalysis from metallic WS₂ nanosheets, *Energy Environ. Sci.* 7 (2014) 2608–2613.
- [36] D. Merki, H. Vrubel, L. Rovelli, S. Fierro, X. Hu, Fe Co, and Ni ions promote the catalytic activity of amorphous molybdenum sulfide films for hydrogen evolution, *Chem. Sci.* 3 (2012) 2515.